1-(9-Anthryl)-3-(1-naphthyl)propane. Crystal and Molecular Structure of the Photoisomer. Photophysics and Photochemistry of the Two Isomers

James Ferguson,*[1a] Albert W-H. Mau,[1b] and Peter O. Whimp[1c]

Contribution from the Research School of Chemistry, The Australian National University, Canberra, Australia. *Received February 3, 1978*

Abstract: The single-crystal X-ray analysis of the photoisomer of 1-(9-anthryl)-3-(1-naphthyl)propane is described. The molecule crystallizes in the monoclinic space group $P2_1/n$ with four molecules per unit cell of dimensions a = 12.686 (4) Å, b = 8.758 (3) Å, c = 17.038 (5) Å, and β = 103.17 (2)°. The conventional R factor for the 2032 reflections of the terminal data with $I/\sigma(I) \geq 3.0$ is 0.037. The bonds formed by the photoisomerization [C(6)-C(26), 1.605 (3) Å; C(13)-C(29), 1.664 (2) Å] are significantly different. The cyclopentane ring is disordered and it has an envelope conformation. Irradiation of the photoisomer photodissociates the molecule and the product appears in its electronically excited (exciplex) state. Polarized fluorescence experiments in viscous solvents show that the exciplex transition moment lies mainly along the short in-plane axis of the anthracene chromophore. Photophysical studies of the more stable isomer have been carried out in rigid glasses, fluid solutions, and the photoisomer crystal, and the effects of conformational arrangement of the two chromophores studied.

Chandross and Schiebel[2] reported the photoisomerization of 1-(9-anthryl)-3-(1-naphthyl)propane (ANP) and single crystals of its photoisomer (ANPPI) were prepared by Puza.[3] A study of the photophysical and photochemical reactions of ANP was made,[3] but an analysis of its absorption spectrum, obtained by the photodissociation of ANPPI in its single crystal, could not be completed because of the lack of crystal structure information.

The present study was undertaken primarily to obtain the necessary crystal and molecular structure information to enable an analysis of the photophysical properties of ANP in ANPPI single crystal. In addition, the photophysical properties of ANP and ANPPI in viscous glasses and fluid solutions were also investigated to determine the effects of temperature and viscosity on the radiationless processes which govern the photochemical behavior of these molecules.

Experimental Section

The preparation of crystals of ANPPI has been given previously[3] and the spectroscopic methods are given in the previous paper.[4] For the present work two solutions of different viscosity were used. These are methylcyclohexane-decalin (1:1, MCH-D) and methylcyclohexane-isopentane (1:3, MCH-IP).

Collection and Reduction of X-ray Intensity Data. Approximate cell dimensions for ANPPI were obtained from preliminary Weissenberg and precession photographs which showed systematic absences ($h0l$ data, $h + l = 2n + 1$; $0k0$ data, $k = 2n + 1$) corresponding to space group $P2_1/n$. [Space group $P2_1/n$ is a nonstandard setting of space group $P2_1/c$ (C_{2h}^5, no. 14)]. The crystal chosen for data collection was transferred to a Picker FACS-1 fully automatic diffractometer, and was aligned with the crystallographic b axis and the instrumental Φ axis approximately coincidental. The unit-cell dimensions (with estimated standard errors), and the crystal orientation matrix were obtained in the usual way.[5] Full details of the crystal data, the data collection method, and experimental conditions used appear in Table I. During data collection, the intensities of the three "standard" reflections showed a regular time-dependent decrease (Table I). Before further calculation, the measured intensities were corrected for anisotropic decay.[6] Reflection intensities were reduced to values of $|F_o|^2$, and each reflection was assigned an individual estimated standard deviation [$\sigma(F_o)$].[6] For this data set, the instrumental "uncertainty" factor[7] (ρ) was set at $(0.002)^{1/2}$. Equivalent reflection forms were averaged, and those reflections with $I/\sigma(I) < 3.0$[6] were discarded as being unobserved. The statistical R factor[6] (R_s) for the 2032 reflections of the terminal data set was 0.019.

Solution and Refinement of the Structure. The structure was solved by direct methods using the MULTAN system of programs.[6] Eight sets of signs for the 250 reflections with $|E| \geq 1.76$ were determined. The E map generated by the chosen starting set showed the positions of the 27 carbon atoms of the molecule. Using data which had been corrected for absorption effects,[8] the structure was refined initially by block-diagonal and, in the latter stages, full-matrix least-squares methods to final unweighted and weighted R factors of 0.037 (R) and 0.049 (R_w), respectively. During least-squares refinement, the minimized function was $\Sigma w(|F_o| - |F_c|)^2$, and individual weights of the form $w = [\sigma(F_o)]^{-2}$ were used throughout: $R = \Sigma||F_o| - |F_c||/\Sigma|F_o|$; $R_w = \{\Sigma w[|F_o| - |F_c|]^2/\Sigma w|F_o|^2\}^{1/2}$; the anisotropic temperature factor was of the form $\exp[-(\beta_{11}h^2 + \beta_{22}k^2 + \beta_{33}l^2 + 2\beta_{12}hk + 2\beta_{13}hl + 2\beta_{23}kl)]$. Scattering factors for carbon atoms were taken from the compilation of Cromer and Mann,[9] and, although the effects were small, the correction for the real and imaginary parts of anomalous scattering was applied.[10,11] Scattering factors for hydrogen atoms were taken from the listing of Stewart et al.[12]

During refinement, we found that one carbon atom was disordered, and the "fractional" atoms C(42A) and C(42B) (see Figure 2) were included in all subsequent least-squares refinement cycles. The occupancy factors for C(42A) and C(42B) were successfully refined to 0.702 (9) and 0.301 (9), respectively. Sixteen isotropic hydrogen atoms were successfully refined, but the hydrogen atoms associated with C(41), C(42A), C(42B), and C(43) were included as fixed contributions to F_c. The fixed hydrogen atom coordinates (assuming C-H = 1.015 Å) and isotropic temperature factors ($B_H = 1.1B_C$ Å^2) were recalculated prior to each refinement cycle. In order to satisfy the disorder problem, we assumed that C(41) and C(43) were each bonded to four hydrogen atoms with occupancy factors corresponding to those found for C(42A) and C(42B).

An extinction correction was applied,[13] and the extinction parameter BO refined successfully to $8.8 \times 10^{-6} \pm 9.8 \times 10^{-7}$.

On the final cycle of least-squares refinement, no individual parameter shift was greater than 0.05 of the corresponding parameter estimated standard deviation. The estimated standard deviation of an observation of unit weight, defined as $[\Sigma w(|F_o| - |F_c|)^2/(m - n)]^{1/2}$ [where m is the number of observations and n (= 320) is the number of parameters varied] was 1.66; cf. an expected value of 1.0 for ideal weighting. There were no unusual features on the final electron-density difference map, and there were no residual maxima greater than 0.2 e/Å^3. A weighting analysis showed that there were no serious trends in the dependence of the minimized function on either $|F_o|$ or $\lambda^{-1}\sin\theta$.

The final atomic positional and thermal parameters, together with their estimated standard deviations (where appropriate), are listed in a table which is available as supplementary material only. Also available as supplementary material is a list of observed and calculated structure factor amplitudes [×10 (electrons)].

Discussion of the Crystal Structure

The crystal structure, as defined by the unit cell parameters, symmetry operations, and atom coordinates,[29] consists of discrete monomeric molecular units which have neither crystallographic nor virtual symmetry higher than C_1. There are no unusually short intermolecular contacts.

0002-7863/79/1501-2370$01.00/0

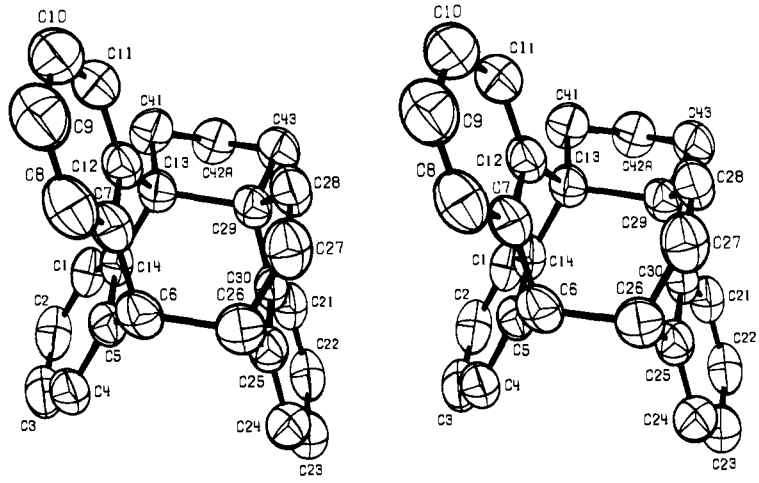

Figure 1. Perspective view of the photoisomer (stereopair) showing the atom number sequence.

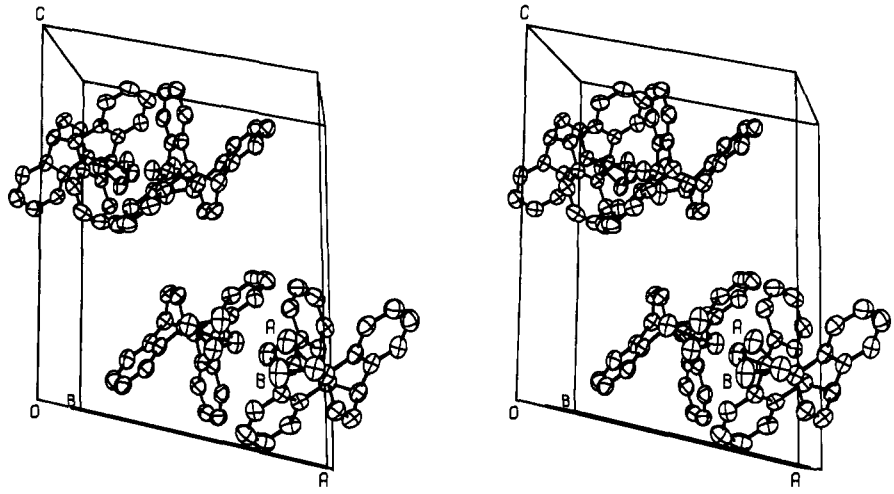

Figure 2. Stereoscopic view of one unit cell, viewed down *a*. The atoms marked A and B show the two possible positions of the disordered atom C(42).

Table I. Crystal Data and Data Collection Details.

radiation: Cu Kα	λ: 1.5418 Å
a = 12.686 (4) Å[a,b]	b = 8.758 (3) Å
c = 17.038 (5) Å	β = 103.17 (2)°
formula: $C_{27}H_{22}$	cell volume: 1843.0 Å^3
ρ_{obsd}: 1.24 (1) g cm^{-3}	ρ_{calcd}: 1.25 g cm^{-3}
μ(Cu Kα): 5.43 cm^{-1}	space group: $P2_1/n$[c]
monochromator: graphite crystal	crystal-counter distance: 28.5 cm
scan method and speed:	θ-2θ scans at 2°/min
scan width:	from 1.15° below the Cu Kα_1 maximum to 1.15° above the Cu Kα_2 maximum
scan range:	$3° \leq 2\theta \leq 124°$
total background count time[d]	20 s
"standard" reflections[e]	(2,0,14); (800); (150)
crystal decomposition[f]	28.78%; 24.28%; 13.92%
total data collected	3397 reflections from the quadrant $hk \pm l$
data with $I/\sigma(I) \geq 3.0$	2032 reflections

[a] Cell dimensions were measured at 20 ± 1 °C. [b] Estimated standard deviations (in parentheses) in this and the following tables, and also in the text, refer to the least significant digit(s) in each case. [c] Space group $P2_1/n$ is a nonstandard setting of space group $P2_1/c[C_{2h}^5$, no. 14]. [d] Backgrounds were recorded on either "side" of each reflection (10 s each side) at the scan width limits, and were assumed to be linear between these two points. [e] The "standard" reflections were monitored after each 100 measurements throughout the course of data collection. [f] The decomposition rates refer respectively to the three "standard" reflections.

A perspective view of one molecule, together with the atom numbering scheme used, is shown by the stereopairs of Figure 1, while the contents of one unit cell and the disorder of C(41) are shown by the stereopairs of Figure 2. In each of these figures the thermal ellipsoids have been drawn to include 50% of the probability distribution, and, for clarity, the hydrogen atoms have been omitted.

Principal bond lengths and interbond angles, together with their estimated standard deviations, are listed in Table II. The results of weighted least-squares planes calculations are collected in Table III.

The overall geometry of the present molecule is very similar to that found for the 9,10-dimethylanthracene-tetracene photodimer[4] and also for the *trans*-ditetracene photodimer.[14] There are, however, some significant geometrical modifications which obviously arise from the presence of the cyclopentane ring C(13)-C(29)-C(43)-C(42)-C(41) in the present molecule.

The effects of π-π repulsion between the "face to face" aromatic rings are shown by the long [cf. the accepted carbon-carbon single bond distance of 1.537 (5) Å][15a] carbon-carbon single bonds which are formed in the photodimerization process. Unlike the previous examples, however, the distances C(6)-C(26) [1.605 (3) Å] and C(13)-C(29) [1.664 (2) Å] are significantly different. The shorter bond [i.e., C(6)-C(26)] is in good agreement with previous observations (i.e., an average value of 1.628 Å for the 9,10-dimethylanthracene-tetracene photodimer[4] and an average of 1.616 Å for *trans*-di-

Table II. Bond Lengths and Interbond Angles

A. Bond Lengths, Å

atoms	distance	atoms	distance	atoms	distance
C(1)-C(2)	1.386 (3)	C(1)-C(14)	1.386 (3)	C(2)-C(3)	1.367 (3)
C(3)-C(4)	1.380 (3)	C(4)-C(5)	1.390 (3)	C(5)-C(14)	1.400 (2)
C(7)-C(8)	1.386 (2)	C(7)-C(12)	1.400 (2)	C(8)-C(9)	1.380 (3)
C(9)-C(10)	1.366 (3)	C(10)-C(11)	1.391 (3)	C(11)-C(12)	1.381 (3)
C(21)-C(22)	1.387 (3)	C(21)-C(30)	1.387 (3)	C(22)-C(23)	1.382 (3)
C(23)-C(24)	1.378 (3)	C(24)-C(25)	1.385 (3)	C(25)-C(30)	1.403 (2)
C(27)-C(28)	1.322 (3)				
C(5)-C(6)	1.509 (3)	C(6)-C(7)	1.505 (3)	C(12)-C(13)	1.539 (2)
C(13)-C(14)	1.528 (2)	C(25)-C(26)	1.506 (3)	C(26)-C(27)	1.499 (3)
C(28)-C(29)	1.512 (3)	C(29)-C(30)	1.525 (3)		
C(13)-C(41)	1.542 (2)	C(41)-C(42A)	1.491 (4)	C(41)-C(42B)	1.546 (9)
C(42A)-C(43)	1.530 (4)	C(42B)-C(43)	1.427 (8)	C(43)-C(29)	1.543 (2)
C(6)-C(26)	1.605 (3)	C(13)-C(29)	1.644 (2)		
C(1)-H(1)	1.00 (2)	C(2)-H(2)	0.98 (2)	C(3)-H(3)	0.98 (2)
C(4)-H(4)	1.00 (2)	C(8)-H(8)	0.97 (2)	C(9)-H(9)	1.01 (2)
C(10)-H(10)	0.97 (2)	C(11)-H(11)	1.01 (2)	C(21)-H(21)	0.99 (2)
C(22)-H(22)	1.02 (2)	C(23)-H(23)	1.01 (2)	C(24)-H(24)	1.02 (2)
C(27)-H(27)	1.00 (2)	C(28)-H(28)	1.03 (2)		
C(6)-H(6)	1.02 (2)	C(26)-H(26)	1.03 (2)		

B. Interbond Angles, deg

atoms	angle	atoms	angle	atoms	angle
C(14)-C(1)-C(2)	120.9 (2)	C(1)-C(2)-C(3)	120.4 (2)	C(2)-C(3)-C(4)	119.8 (2)
C(3)-C(4)-C(5)	120.5 (2)	C(4)-C(5)-C(14)	120.0 (2)	C(4)-C(5)-C(6)	122.2 (2)
C(6)-C(5)-C(14)	117.8 (2)	C(5)-C(14)-C(1)	118.4 (2)	C(5)-C(14)-C(13)	117.4 (2)
C(1)-C(14)-C(13)	124.2 (2)	C(6)-C(7)-C(8)	122.5 (2)	C(6)-C(7)-C(12)	117.7 (2)
C(12)-C(7)-C(8)	119.8 (2)	C(7)-C(8)-C(9)	121.1 (2)	C(8)-C(9)-C(10)	119.4 (2)
C(9)-C(10)-C(11)	120.1 (2)	C(10)-C(11)-C(12)	121.4 (2)	C(11)-C(12)-C(7)	118.2 (2)
C(11)-C(12)-C(13)	124.4 (2)	C(7)-C(12)-C(13)	117.4 (2)	C(30)-C(21)-C(22)	121.0 (2)
C(21)-C(22)-C(23)	120.3 (2)	C(22)-C(23)-C(24)	119.7 (2)	C(23)-C(24)-C(25)	120.4 (2)
C(24)-C(25)-C(30)	120.6 (2)	C(24)-C(25)-C(26)	122.1 (2)	C(26)-C(25)-C(30)	117.2 (2)
C(25)-C(30)-C(21)	118.1 (2)	C(25)-C(30)-C(29)	116.8 (2)	C(21)-C(30)-C(29)	125.2 (2)
C(26)-C(27)-C(28)	118.0 (2)	C(27)-C(28)-C(29)	119.9 (2)		
C(5)-C(6)-C(7)	107.0 (2)	C(5)-C(6)-C(26)	113.3 (2)	C(7)-C(6)-C(26)	113.0 (2)
C(12)-C(13)-C(14)	105.5 (1)	C(12)-C(13)-C(29)	111.5 (1)	C(12)-C(13)-C(41)	113.0 (2)
C(14)-C(13)-C(29)	110.9 (1)	C(14)-C(13)-C(41)	113.5 (2)	C(29)-C(13)-C(41)	102.6 (1)
C(25)-C(26)-C(27)	108.1 (2)	C(25)-C(26)-C(6)	110.8 (2)	C(27)-C(26)-C(6)	111.3 (2)
C(28)-C(29)-C(30)	107.6 (2)	C(28)-C(29)-C(13)	110.8 (1)	C(28)-C(29)-C(43)	111.4 (2)
C(30)-C(29)-C(13)	111.4 (1)	C(30)-C(29)-C(43)	112.8 (2)	C(43)-C(29)-C(13)	103.0 (1)
C(13)-C(41)-C(42A)	106.8 (2)	C(13)-C(41)-C(42B)	102.9 (3)	C(41)-C(42A)-C(43)	101.9 (2)
C(41)-C(42B)-C(43)	104.2 (6)	C(42A)-C(43)-C(29)	105.3 (2)	C(42B)-C(43)-C(29)	105.5 (3)

tetracene[14]), while the longer bond [C(13)-C(29)] is in the sterically strained (see below) cyclopentane ring.

As expected, the distance between the centers of gravity of the "face to face" aromatic rings (3.57 Å) is in good agreement with the accepted van der Waals "thickness" of an aromatic ring (ca. 3.6 Å). In contrast, the nonbonded distances C(5)···C(25) (2.74 Å), C(7)···C(27) (2.74 Å), C(12)···C(28) (2.76 Å), and C(14)···C(30) (2.77 Å) are short, but they are in excellent agreement with the corresponding distances found for the 9,10-dimethylanthracene-tetracene adduct (average 2.74 Å)[4] and also for a number of cyclophane derivatives (ca. 2.7-2.8 Å),[16] and are indicative of considerable π-π repulsion.

Within the three aromatic rings of the molecule, the geometry is normal. Thus, the carbon-carbon distances [range 1.366 (3)-1.403 (2) Å] average 1.385 Å, the internal C-C-C ring angles average 120.0°, the mean C-H distance is 1.00 Å, and there are no significant trends in the deviations of the aromatic carbon and hydrogen atoms from their respective ring planes (Table III).

The bond C(27)-C(28) is a simple double bond, and the observed distance of 1.322 (3) Å is in good agreement with the accepted value of 1.335 (5) Å.[15b] The angles C(26)-C(27)-C(28) [118.0 (2)°] and C(27)-C(28)-C(29) [119.9 (2)°] are close to the expected value of 120.0°, and the four atoms C(26), C(27), C(28), and C(29) are planar within experimental error (Table III).

The distances C(5)-C(6) [1.509 (3) Å], C(6)-C(7) [1.505 (3) Å], C(25)-C(26) [1.506 (3) Å], C(26)-C(27) [1.499 (3) Å], and C(28)-C(29) [1.512 (3) Å] are within experimental error of the value of 1.505 Å[15b] expected for single bonds between sp^2- and sp^3-hybridized carbon atoms.

The cyclopentane ring, which is disordered (see Figure 2), has an envelope conformation, and the atoms C(13), C(29), C(41), and C(43) are approximately planar (see Table III). The disorder arises from the position of the fifth atom relative to the remaining four. In the major isomer (70% of the crystal examined), C(42A) is directed toward the "face to face" phenyl rings. Both conformations of the cyclopropane ring are sterically strained. In addition to the abnormally long carbon-carbon bond [C(13)-C(29)] (see above), and compression of the bonds C(41)-C(42A) and C(42B)-C(43) [1.491 (4) and 1.427 (8) Å, respectively], the internal ring angles (at C(13) [102.6 (1)°], C(29) [103.0 (1)°], C(41) [average 104.8°], C(42A) [101.9 (2)°], C(42B) [104.2 (6)°], and C(43) [average 105.4°]) are all significantly smaller than the regular tetrahedral angle.

Photophysics of ANP and ANPPI in Solution

The photophysical properties of ANP depend on the con-

Table III. Least-Squares Planes

A. Best Weighted Least-Squares Planes

plane	atoms defining plane	equation[a]
1	C(1), C(2), C(3), C(4), C(5), C(14)	$-0.8030X - 0.4582Y - 0.3688Z + 8.5733 = 0$
2	C(7), C(8), C(9), C(10), C(11), C(12)	$0.7069X + 0.4607Y - 0.5367Z - 3.7802 = 0$
3	C(21), C(22), C(23), C(24), C(25), C(30)	$0.7168X + 0.4927Y - 0.4933Z - 2.7465 = 0$
4	C(27), C(27), C(28), C(29)	$-0.8410X - 0.4425Y - 0.3114Z + 6.9583 = 0$

B. Deviations (Å) of Atoms from Best Planes

atom	plane 1	atom	plane 2	atom	plane 3	atom	plane 4
C(1)	0.001 (2)	C(7)	−0.001 (2)	C(21)	0.006 (3)	C(26)	0.000 (2)
C(2)	−0.008 (3)	C(8)	0.002 (2)	C(22)	0.004 (2)	C(27)	0.000 (2)
C(3)	0.005 (3)	C(9)	0.001 (3)	C(23)	−0.009 (2)	C(28)	0.000 (2)
C(4)	0.003 (2)	C(10)	−0.005 (3)	C(24)	0.000 (2)	C(29)	0.000 (2)
C(5)	−0.005 (2)	C(11)	0.004 (2)	C(25)	0.007 (2)	H(27)	−0.04 (2)
C(14)	0.003 (2)	C(12)	−0.001 (2)	C(30)	−0.009 (2)	H(28)	−0.08 (2)
C(6)	−0.074 (2)	C(6)	0.021 (2)	C(26)	0.030 (2)		
C(13)	−0.013 (2)	C(13)	0.038 (2)	C(29)	−0.063 (2)		
H(1)	−0.04 (2)	H(8)	0.02 (2)	H(21)	0.01 (2)		
H(2)	−0.08 (2)	H(9)	0.02 (2)	H(22)	−0.07 (2)		
H(3)	0.01 (2)	H(10)	0.02 (2)	H(23)	0.07 (2)		
H(4)	0.04 (2)	H(11)	0.04 (2)	H(24)	−0.04 (2)		

[a] The equations $LX + MY + NZ + D = 0$ refer to orthogonal coordinates, where $X = 12.6855x + 0.0y - 3.8823z$; $Y = 0.0x + 8.7576y + 0.0z$; $Z = 0.0x + 0.0y + 16.5895z$.

Table IV. Arrhenius Parameters for Thermal Quenching of ANP Fluorescence

solvent	A, s^{-1}	$E^{\ddagger}$, kcal mol^{-1}
MCH-IP	1.5×10^{11}	3.8
MCH-D	6.3×10^{11}	5.1

formational arrangement of its two chromophores. Some control over the molecular conformation can be achieved by photochemically generating ANP from ANPPI in a rigid glass, so that the constraints of the solvent cage hold the chromophores in a face to face arrangement. However, as this is not the normal ground-state conformation, the resulting interchromophore relationships are entirely determined by the microstructure of the cage and softening of the glass allows them to move apart.

Earlier measurements[3] were made in methylcyclohexane at 77 K and higher, by absorption spectrophotometry. In the present work, MCH-D was used because of its very high viscosity. Photodissociation was carried out below 77 K and the products were then detected by the excitation spectrum technique, so that the effect of strain on the transmission properties of the glass (base-line shift) was eliminated. The glass was then warmed and the spectrum measured to determine the effect of thermal relaxation and this procedure was repeated until the solvent was no longer rigid. Some representative results are given in Figure 3 for which the photodissociation temperature was 45 K. At this temperature the ANP molecules are locked in a face to face conformation and the excitation spectrum shows a very significant shift of the chromophore levels to low energy as a result of the overlap enforced by the cage. These shifts are not equal (see Figure 3), so they are not all dominated by a (repulsive) destabilization of the ground state. Increasing the temperature of the glass allows the ground state to relax, progressively, and the energy levels shift upward toward those of the normal ground-state conformation.

The fluorescence spectrum of ANP in its normal ground state has been studied previously[3,17] and it is associated almost completely with the anthracene chromophore. As with other 9-substituted anthracenes the fluorescence yield is dependent on temperature and solvent viscosity.[18] The excitation technique was used to measure this dependence on temperature in two solvents of different viscosity. The 0,*n* (n = 0, 1, 2, 3) vibronic bands in these spectra were then used as measures of the fluorescence yield and the results are given in Figure 4. These results show that the temperature-dependent quenching of the ANP fluorescence sets in at about 180 K for MCH-IP and at about 230 K for MCH-D. The data provide good Arrhenius plots according to the relation

$$1/\phi_f - 1 = A \exp(-E^{\ddagger}/RT)$$

and the values of A and $E^{\ddagger}$ are given in Table IV.

Additional information can be obtained from measurements of the fluorescence polarization as a function of temperature. The results, for the 0,0 and 0,1 bands of ANP in MCH-IP, are given in Figure 5. They show that the onset of depolarization

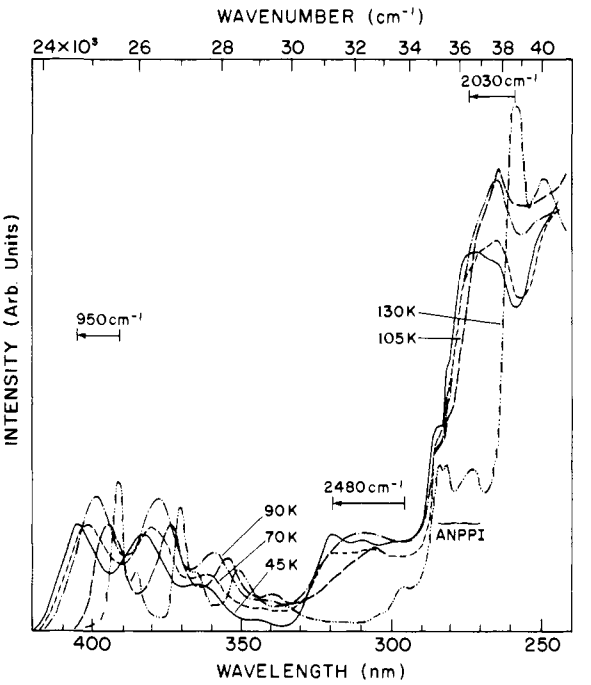

Figure 3. Excitation spectra of ANPPI in MCH-D, taken at 45 K, after 254-nm irradiation, and higher temperatures. The contribution from ANPPI is enclosed by curly brackets and the remainder is due to ANP in various stages of relaxation.

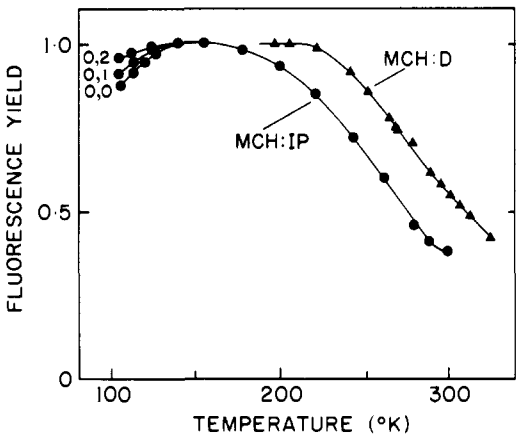

Figure 4. Fluorescence yield of ANP at various temperatures in MCH-D and MCH-IP. The yields were measured by an excitation spectrum technique using the vibronic maxima of the anthracene and naphthalene chromophores. Below about 130 K there are apparent changes in the yield, due to broadening effects (0,0; 0,1; 0,2 of the anthracene chromophore; see text).

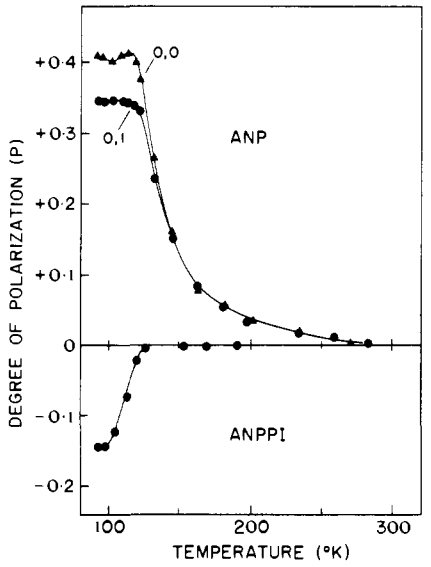

Figure 5. Upper: degree of polarization (P) of the fluorescence of ANP in MCH-IP at various temperatures, for the excitation in the 0,0 and 0,1 bonds of the anthracene chromophore. Lower: degree of polarization (P) of the fluorescence of ANPPI in MCH-IP at various temperatures, for excitation in the 285-nm band of ANPPI.

is at about 120 K. However, below this temperature there is a significant variation of the degree of polarization[19] (P) of the 0,0 band. Between 90 and 120 K P falls, rises to a maximum, and then drops again with increasing temperature. Over the same range of temperature there is a change of the line widths of the bands, greatest for the 0,0 band, which increase below about 125 K. These are reflected in the peak intensities, shown in Figure 4. The broadening of the absorption bands below 125 K is a curious feature which reflects an increase in the inhomogeneity of the sites available for ANP in the glass, brought about by some change in the physical properties of the glass. It is possible that this involves a freezing in of internal rotational motions of the solvent molecules so that the excitation energies of the ANP molecule are no longer determined by a time average of the interactions with the solvent molecules.

The polarization measurements therefore clearly indicate that the onset of ANP molecular rotation, during the lifetime of the excited state, is at about 120 K. Below this temperature

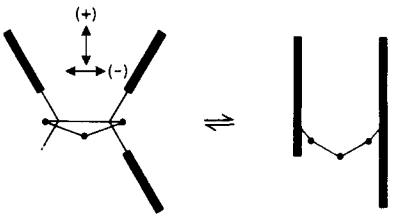

Figure 6. Schematic diagram showing photoisomerization of ANP (right) and photodissociation of ANPPI (left). The transition moment directions of the in-phase (+) and out of phase (−) combinations of the electronic transitions derived from benzene $^1A_{1g} \rightarrow {}^1B_{2u}$ for the two facing benzene chromophores in the ANPPI molecule are shown by the arrows.

there are more subtle changes which involve the glass structure in a different way. Unfortunately, very little is known about the physical properties of glass-forming solvents over a wide range of temperature, the measurements of Greenspan and Fischer[20] being confined to relatively narrow temperature ranges. Hilpern et al.[21] have determined the viscosity of isopentane between 77 K and room temperature and they found a sharp change in gradient for the relationship between log viscosity and reciprocal temperature at about 145 K. They concluded that at this temperature there is a change in the mechanism of viscous flow.

The onset of fluorescence quenching of ANP in MCH-IP is near 180 K while in MCH-D it is about 230 K. In addition, the onset of the thermal dissociation of the exciplex generated by irradiation of ANPPI in these solvents occurs at exactly the same temperature as the onset of fluorescence quenching. It is evident that there is some common physical property of the solvent involved in each case and it seems likely that it is the change in the mechanism of viscous flow, noticed by Hilpern et al.[21] The addition of the more viscous MCH to IP could very well raise the temperature of this change from 145 to 180 K.

One theory[22] of viscosity uses the concept of holes in the liquid. Perhaps the volume of such holes needs to reach a critical size before molecular motion into the holes becomes a significant factor in viscous flow. If so, the average volume of the hole will depend on the temperature and the temperatures noted above might correspond to the holes attaining this critical size. As well as the dissociation of the exciplex at these temperatures it is reasonable that the change in the mechanism of viscous flow controls the probability of various intramolecular motions which, in turn, govern the radiationless internal conversion of the electronic excitation energy. Out of plane motions of the anthracene chromophore would be likely candidates in this regard.

Similar polarization experiments were carried out with ANPPI in MCH-IP and the degree of polarization of the (exciplex) fluorescence[23] is also shown in Figure 5. P is negative and depolarization sets in at about 100 K and is complete by 125 K.

We examine the sign of P first. The absorption of light takes place in the benzene chromophore system of ANPPI. The two facing benzene chromophores (see Figure 6) interact and their energy levels will lie lower in energy than that of the third benzene chromophore. The two lowest energy maxima in the absorption spectrum of ANPPI (enclosed by curly brackets in Figure 3) therefore probably correspond to the in-phase (+) and out of phase (−) components of the coupled pair. The transitions to these states have their parentage in the $^1A_{1g} \rightarrow {}^1B_{2u}$ transition of benzene so that the polarization directions for the pair will be as shown in Figure 6.

The exciplex emission generated by irradiation of the ANPPI comes from the photodissociated product molecule ANP.[23] As the dissociation occurs in a rigid medium, the product molecule retains its topochemical relationship to the

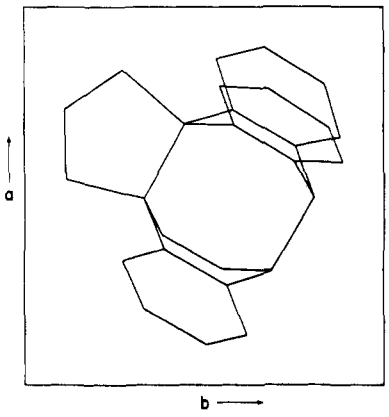

Figure 7. Projection of the ANPPI molecule on to the well-developed face (001) of the crystal.

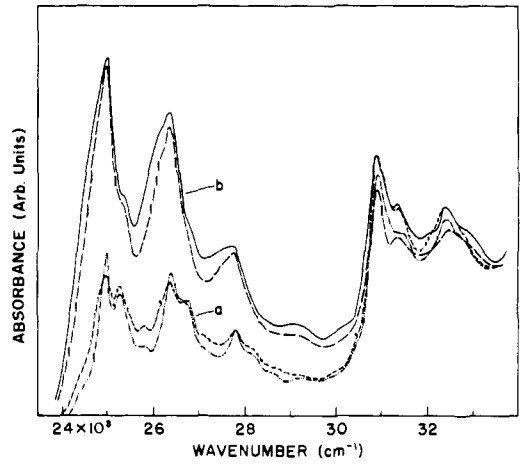

Figure 8. Absorption by ANP in ANPPI crystal in polarized light for light incident on the (001) face of the crystal. (b) is for the electric vector ‖**b** and (a) is for the electric vector ‖**a**. One set of spectra (b, — and a, - - -) was measured immediately after photodissociation at 10 K by 290-nm light. The other set (b, - - -, a, — . . —) was measured at 10 K, after the crystal had been taken to about 150 K for a few minutes.

ANPPI molecule (see Figure 6) and the fluorescence will be polarized. Its negative P indicates that the emitting transition moment is orthogonal to the directions in Figure 6, i.e., normal to the plane of the paper and along the short in-plane axis of the anthracene chromophore. The polarization ratio does not have the minimum possible value of $-\frac{1}{3}$, however. This means that either the emitting moment is not exactly orthogonal to the absorption moments or there is partial rotation of the product molecule during its excited state. A combination of both factors could also be responsible.

The depolarization of the exciplex fluorescence is complete by 125 K, in contrast to the case of the ANP fluorescence considered above. The lifetime of the exciplex under these conditions is about 37 ns, about three times longer than that for the normal conformation of ANP. Therefore, rotational diffusion will lead to a more rapid depolarization of the exciplex fluorescence, but the difference is not enough to explain the observed behavior. It seems more likely that the depolarization occurs because the dissociated product is "hot" and much of its excess energy is dissipated through rotational motion. In this respect it is perhaps significant that the depolarization is complete close to the temperature at which the onset of rotational motion is observed through the depolarization of the 0,0 band of ANP. Also, the depolarization occurs over the range of temperature for which line-width changes in the ANP spectrum were observed, possibly associated with the internal rotational motions of the solvent molecules.

Measurements of the total fluorescence intensity excited from the ANPPI at various temperatures reveal that the total intensity (exciplex plus the dissociated exciplex) is quenched above about 240 K in MCH-D. It is likely that the main contribution to this quenching comes from the dissociated exciplex fluorescence, considered above. However, the exciplex fluorescence is also quenched by the temperature-dependent photoisomerization and the rate of the dissociation of the exciplex is also temperature dependent, so that the overall fluorescence yield involves a complicated rate expression which is beyond the scope of the present work. In any case it will be necessary to carry out time-resolved experiments in the subnanosecond region before a detailed understanding of these excited-state reactions can be obtained. These are planned and they should also provide a value for the exciplex stabilization energy, which, on present evidence, appears to be small.

Absorption by ANP in ANPPI Crystal

The technique[24] of generating the photodissociated products of photodimers and photoisomers in their respective crystals was used previously[3] to determine the absorption and fluorescence spectra of ANP in ANPPI. Since then, further work[25,27] has established that the wavelength used for photodissociation and the temperature of the crystal are very important experimental variables. In the earlier work, the photodissociation was carried out at room temperature while in the present work low temperatures (~10 K) were used.

The well-developed face of the ANPPI crystal is (001) and the projection of the molecule on this face is given in Figure 7. Irradiation of the crystal with ultraviolet light photodissociates the ANPPI molecule and ANP is the product. This molecule must then adjust to the constraints imposed by the ANPPI lattice but it appears that the molecule can adopt a variety of conformations. The reason for this is probably the disparity in the sizes of the naphthalene and anthracene chromophores, so that the position of the former relative to the latter is not well defined by the lattice. The corresponding spectra overlap appreciably and a detailed quantitative analysis of the absorption spectrum is not possible, so we are limited to a more qualitative discussion.

To illustrate the complexity of the absorption spectrum of the photodissociation products we show in Figure 8 the spectrum obtained after irradiation of a single crystal of ANPPI with 290-nm light at 10 K, together with the spectrum after the crystal temperature had been raised to about 150 K for a few minutes and then taken back to 10 K. The wavelength of the photodissociating light is on the absorption edge, so the concentration of ANP molecules is low. In spite of this there is a thermally induced relaxation which alters the distribution among the various conformations. In the region of the naphthalene chromophore absorption (>30 500 cm^{-1}), there is an overall decrease of absorption intensity. However, for the anthracene chromophore, the band system with origin at 25 000 cm^{-1} shows an increase of absorption intensity at the expense of bands with origins <25 000 cm^{-1}. This behavior is in general qualitative agreement with the thermal relaxation experiments in rigid glasses described above. We therefore associate the presence of the naphthalene chromophore absorption with conformations which have absorption by the anthracene chromophore displaced the furthest toward low energy.

The behavior, illustrated in Figure 8, varies somewhat from crystal to crystal, some showing more effects of thermal relaxation, some less. This no doubt reflects variations in the homogeneity of the internal structures of these solution-grown crystals, so that the data in Figure 8 illustrate qualitatively the

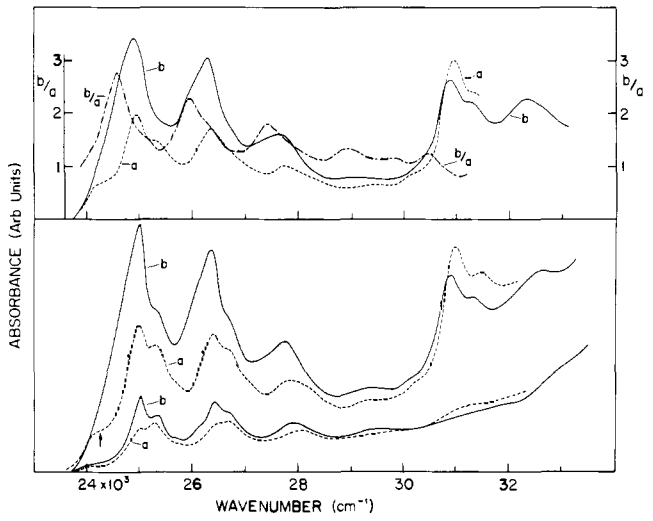

Figure 9. Lower: top two curves measured after irradiation of single crystal of ANPPI by 254-nm light at 10 K. (a) and (b) correspond to electric vector parallel to (a) and (b), respectively, for light incident on the (001) face. Bottom two curves measured at 10 K, after room temperature irradiation with 24 250-cm^{-1} light (arrow) at room temperature. Upper: (a) and (b) are the different spectra obtained by subtracting the two bottom curves from the two upper curves in the bottom panel. The polarization ratio (b/a) is given by the dotted line.

variation in the absorption spectra of the photodissociation products.

In addition to changes brought about by thermal relaxation, it is possible to remove a large fraction of the remaining molecules photochemically through photoisomerization, leaving the most relaxed or photoresistant conformations to be studied separately. The results of this type of experiment are given in Figure 9. The bottom panel shows the 10 K absorption spectra immediately after photodissociation at 10 K by 254-nm light, together with the spectra (at 10 K) taken after the crystal had been irradiated, at the wavelength corresponding to the arrow (24 250 cm^{-1}), at room temperature. The difference spectra are given in the upper panel and therefore contain the overlapping spectra of the readily photoisomerizable conformations. The presence of more than one conformation is indicated by the varying polarization ratio, included in the upper panel of Figure 9.

Let us estimate the expected polarization ratio for the ANP molecule by assuming a symmetrical dissociation of the ANPPI molecule to give interplanar contacts of about 3.5 Å. We find that the ^1L_a band of the anthracene chromophore should have a b/a ratio of about 4:1, while the ^1L_a band of the naphthalene chromophore should have a b/a ratio of about 2:1. If the interplanar contacts are made less than 3.5 Å both ratios will move toward 3:1.

From Figure 9, upper panel, we see that the ^1L_a band of the naphthalene chromophore has a b/a ratio less than 1 and there are regions of the ^1L_a band of the anthracene chromophore for which the ratio approaches 1. The origin of the latter is on the low-wavenumber edge, near 24 800 cm^{-1}, corresponding to the most constrained conformation.

The low b/a values can have two possible explanations. They can arise either because the ANP molecule adjusts to the lattice constraints by a small rotation (clockwise) about an axis normal to the plane of Figure 7, or because of a change in the mechanism of the absorption of light. The latter would be the result of the interaction between the two chromophores. The first is unlikely because rotation implies a degree of relaxation, inconsistent with the requirement of rigid lattice constraint. We are left therefore with the second explanation.

The most important interaction between the two chromophores comes from orbital overlap, forced by the constraints of the lattice. The energy states of each chromophore are then contaminated by admixtures of charge-transfer states, which can be either from the naphthalene to the anthracene or vice versa (highest occupied MO to lowest unoccupied MO in each case). The incorporation of these charge-transfer states will have the effect of moving the transition moments for the ^1L_a bands out of the corresponding molecular planes. Relatively small admixtures of out of plane components would account for the observed polarization ratios.

This explanation is speculative but it is in line with a theoretical model[28] developed to interpret the fluorescence from exciplexes and mixed excimers. In this approach the transition moment matrix elements are couched in terms of localized and charge transfer transition moments, using first-order perturbation theory. However, it is clear that a detailed theoretical understanding of the quantitative effects of overlap on the energy levels and transition moments of ANP will require a more complex approach. For example, the observed decay time of the exciplex fluorescence is 80 ns,[3] about five times larger than the decay time of the anthracene chromophore emission. This implies a relatively large admixture of a charge-transfer state into the emitting state of the exciplex and yet the polarization ratio of the fluorescence (b/a = 1.5) implies a major in-plane component in the exciplex transition moment. Also, we can note that the absorption intensity of the ^1L_a band of the naphthalene chromophore is relatively larger in the rigidly constrained ANP than is the case for the relaxed ANP (see Figure 3). In both cases there are significant changes from the localized transition properties, as a result of the enforced overlap, so that the actual electron density changes brought about by charge-transfer interactions might be outside the scope of first-order perturbation theory.

The ability to observe the energy levels of the two chromophores under conditions of enforced overlap is a very attractive feature of the present technique. It is unfortunate, however, that the orientation of the ANP molecule does not allow a measure of the polarized intensity along the long axes of the chromophores, in order to observe the effect of overlap on the ^1L_b bands. In this regard the crystal of the photoisomer of 1,3-di(9-anthryl)propane has a habit and structure which allows discrimination between short and long in-plane molecular axes. Hydrogenation of one of the anthracene chromophores at its 1, 2, 3, and 4 positions produces a naphthalene chromophore analogous to ANP. Incorporation of the photoisomer of this compound into the crystal of the photoisomer of the dianthrylpropane enables the selective photodissociation of the former so that the ^1L_a bands can be measured. These spectra show that the ^1L_a band of the anthracene chromophore has its intensity enhanced through the enforced overlap and the origin band of the ^1L_a system has significant long-axis polarization. On this evidence it is possible that the exciplex emitting state represents an admixture of ^1L_a, ^1L_b, and charge-transfer states. If this is the case then the long decay time can be seen to be a result of the importance of the last two states in the exciplex. This aspect is being pursued at present.

Fluorescence from ANP in ANPPI Crystal

The exciplex nature of the fluorescence from photodissociated ANPPI was demonstrated earlier.[2,3] In the present paper we consider, instead, the fluorescence emitted from those molecules which have relaxed away from the photoisomerizable conformations. The spectra in Figure 10 are then typical of the absorption spectra of the photostable molecules. There are two main conformations, one with origin at 25 000 cm^{-1} and the other with its origin at 25 350 cm^{-1}. The latter is very close to the position expected for the normal ground-state conformation of ANP so it is not surprising that irradiation with light in this region gives rise to structured fluorescence, characteristic of the anthracene chromophore.

The range of conformations can be probed by using narrow-band excitation to generate a series of fluorescence spectra. When this is done it is found that the features of the fluorescence spectrum change continuously from a structured spectrum through to a continuous exciplex spectrum as shown in Figure 10. The range of conformations is determined by the distribution of sites for the ANP molecules, presumably related to the concentration gradient through the crystal caused by the exponential absorption of the photodissociating light. The greater the concentration the more disruption to the lattice and larger the relaxation away from the topochemical conformation.

Each conformation has its individual emission spectrum and there is no evidence to suggest that equilibration to a common excited-state conformation occurs. However, there is evidence (Figure 10) to show that the gap between the electronic transitions in the absorption and fluorescence spectra widens as the exciting wavelength moves to lower energy. This indicates that the molecules relax to energetically more stable positions after excitation. Most likely this involves a closer approach of the two chromophores in a partially overlapped face to face conformation as this is the only motion allowed by the lattice constraints; otherwise a common fluorescence spectrum would be observed.

The stabilization of the excited state is due to the charge-transfer interaction between the two chromophores and is therefore directly related to the overlap of the two π-electron systems. The greater the overlap, the larger the gap and there is a continuous range of conformations from zero to complete overlap.

Turning to Figure 10 we note that excitation at 4, 5, and 6 provides a marked change in the fluorescence spectra, even though these positions are close together. Also, the absorption maximum at 25 000 cm^{-1} is associated with a group of conformations whose emission spectra retain a very broad, red-shifted structured component (spectra 2 and 3), while spectrum 1 is essentially the true exciplex emission.

The smooth change from structured fluorescence to exciplex fluorescence, evident in Figure 10, is in qualitative agreement with overlap dependent charge-transfer nature of the excited-state interactions, as described by Beens and Weller.[28]

The gap between absorption and fluorescence spectra points to a change in the interchromophore separation after excitation and establishes the charge-transfer contribution to the exciplex stabilization energy. As the gap widens the vibrational structure broadens and the Franck-Condon intensity maximum shifts to the red. The broadening of the structure can, in part, be described as inhomogeneous broadening, but the shift of intensity cannot. It points to a change in the nature of the electron-nuclear coupling in the exciplex. This change is brought about by an alteration of the electron-density distribution in the exciplex as a result of the charge transfer. The two chromophores are, of course, closer together in the exciplex than in the ground state and the significant configuration coordinate is in the direction from one chromophore to the other. The energy dependences of the ground and exciplex states are grossly different along this coordinate; the former is repulsive while the latter is attractive and the continuous nature of the fluorescence intensity distribution follows immediately. The electronic transition density change is not, however, in this direction, although it is likely that there is a component along this direction as discussed above.

Acknowledgments. We are grateful for generous allocations of time on the Univac-1108 computer at The Australian National University Computer Centre.

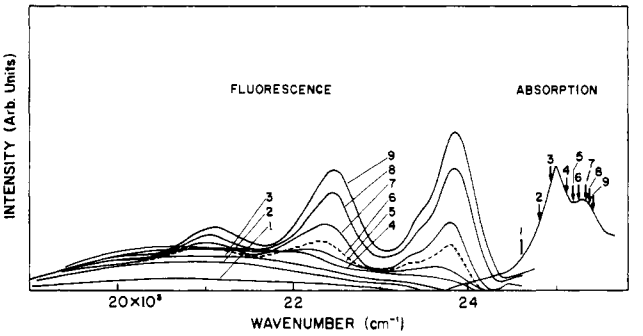

Figure 10. Fluorescence spectra (1, ... 9; left) measured for irradiation at the arrow position (1, ... 9; right) of the absorption spectrum, at 10 K. The crystal was the same as described in Figure 9.

Supplementary Material Available. A listing of structure factor amplitudes (13 pages). Ordering information is given on any current masthead page.

References and Notes

(1) (a) Research School of Chemistry, Australian National University. (b) Division of Applied Organic Chemistry, C.S.I.R.O., P.O. Box 4331, G.P.O. Melbourne, Victoria 3001, Australia. (c) Physics & Engineering Laboratory, D.S.I.R., Private Bag, Lower Hutt, New Zealand.
(2) E. A. Chandross and A. H. Schiebel, *J. Am. Chem. Soc.*, **95**, 1671-1672 (1973).
(3) J. Ferguson, A.W-H. Mau, and M. Puza, *Mol. Phys.*, **28**, 1457-1466 (1974).
(4) J. Ferguson, A.W-H. Mau, and P. O. Whimp, *J. Am. Chem. Soc.*, preceding paper in this issue.
(5) The programs contained in the Picker Corp. FACS-I Disk Operating System (1972) were used for all phases of diffractometer control and data collection.
(6) All calculations were carried out on the Univac-1108 computer at The Australian National University Computer Centre using the ANUCRYS system of crystallographic programs. A description of ANUCRYS, including relevant formulas, has appeared in ref 4.
(7) W. R. Busing and H. A. Levy, *J. Chem. Phys.*, **26**, 563-568 (1957); P. W. R. Corfield, R. J. Doedens, and J. A. Ibers, *Inorg. Chem.*, **6**, 197-204 (1967).
(8) Distances to the crystal boundary faces from the arbitrarily chosen crystal "origin" follow: {001}, 0.006 cm; {001}, 0.006 cm; {101}, 0.013 cm; {101}, 0.013 cm; {110}, 0.021 cm; {110}, 0.023 cm; {232} 0.018 cm. The transmission factor, applied to $|F_o|$, ranged from 0.916 to 0.972.
(9) D. T. Cromer and J. B. Mann, *Acta Crystallogr., Sect. A*, **24**, 321-324 (1968).
(10) C. T. Prewitt, Ph.D. Thesis, Massachusetts Institute of Technology, 1962, p 163.
(11) D. T. Cromer and D. Liberman, *J. Chem. Phys.*, **53**, 1891-1898 (1970).
(12) R. F. Stewart, E. R. Davidson, and W. T. Simpson, *J. Chem. Phys.*, **42**, 3175-3187 (1965).
(13) The secondary extinction correction was applied to F_c as $F_c/(1.0 + EXT1 \times EXT2 \times BO)$ (where EXT1 and EXT2 are the reflection intensity and the Zachariasen "β" factor, respectively, and BO is refined). For additional details, see W. H. Zachariasen, *Acta Crystallogr.*, **16**, 1139-1144 (1963).
(14) J. Gaultier, C. Hauw, J. P. Desvergne, and R. Lapouyade, *Cryst. Struct. Commun.*, **4**, 497-500 (1975).
(15) *Chem. Soc., Spec. Publ.*, **No. 18** (1965); (a) p S14s; (b) p S15s.
(16) D. J. Cram and J. M. Cram, *Acc. Chem. Res.*, **4**, 204-213 (1971).
(17) O. Schnepp and M. Levy, *J. Am. Chem. Soc.*, **84**, 172-177 (1962).
(18) E. J. Bowen and J. Sahu, *J. Phys. Chem.*, **63**, 4-7 (1959).
(19) A. C. Albrecht, *J. Mol. Spectrosc.*, **6**, 84-108 (1961).
(20) H. Greenspan and E. Fischer, *J. Phys. Chem.*, **69**, 2466-2469 (1965).
(21) J. W. Hilpern, G. Porter, and C. J. Stief, *Proc. R. Soc. London, Ser. A*, **277**, 437-447 (1964).
(22) S. Glasstone, K. Laidler, and H. Eyring, "Theory of Rate Processes," McGraw-Hill, New York, 1941, Chapter 9.
(23) J. Ferguson and M. Puza, *Chem. Phys. Lett.*, **53**, 215-218 (1978).
(24) J. Ferguson and A.W-H. Mau, *Mol. Phys.*, **27**, 377-387 (1974).
(25) J. Ferguson and S. E. H. Miller, *Chem. Phys. Lett.*, **36**, 635-638 (1975).
(26) J. Ferguson, M. Morita, and M. Puza, *Chem. Phys. Lett.*, **42**, 288-282 (1976).
(27) J. Ferguson, M. Morita, and M. Puza, *Chem. Phys. Lett.*, **49**, 265-268 (1977).
(28) H. Beens and A. Weller, "Organic Molecular Photophysics," Vol. 2, J. B. Birks, Ed., Wiley, New York, 1975, pp 159-215.
(29) Please refer to the table in supplementary material.